

Maximum Diameter of Impacting Liquid Droplets

Nick Laan,¹ Karla G. de Bruin,² Denis Bartolo,³ Christophe Josserand,⁴ and Daniel Bonn¹

¹*Van der Waals-Zeeman Institute, Institute of Physics, University of Amsterdam, Science Park 904, 1098 XH Amsterdam, Netherlands*

²*Netherlands Forensic Institute, The Hague, Netherlands*

³*Ecole Normale Supérieure de Lyon, CNRS UMR 46 allé d'Italie, 69007 Lyon, France*

⁴*Institut D'Alembert, UMR 7190 CNRS and UPMC (Université Paris 6), 4 place Jussieu, 75006 Paris, France*

(Received 18 February 2014; revised manuscript received 6 October 2014; published 30 October 2014)

The maximum diameter a droplet that impacts on a surface will attain is the subject of controversy, notably for high-velocity impacts of low-viscosity liquids such as water or blood. We study the impact of droplets of simple liquids of different viscosities, and a shear-thinning complex fluid (blood), for a wide range of surfaces, impact speeds, and impact angles. We show that the spreading behavior cannot simply be predicted by equating the inertial to either capillary or viscous forces, since, for most situations of practical interest, all three forces are important. We determine the correct scaling behaviors for the viscous and capillary regimes and, by interpolating between the two, allow for a universal rescaling. The results for different impact angles can be rescaled on this universal curve also, by doing a simple geometrical correction for the impact angle. For blood, we show that the shear-thinning properties do not affect the maximum diameter and only the high-shear rate viscosity is relevant. With our study, we solve a long-standing problem within the fluid-dynamics community: We attest that the spreading behavior of droplets is governed by the conversion of kinetic energy into surface energy or dissipated heat. Energy transfer into internal flows marginally hinders droplet spreading upon impact.

DOI: [10.1103/PhysRevApplied.2.044018](https://doi.org/10.1103/PhysRevApplied.2.044018)

I. INTRODUCTION

Controlling droplet deposition is of great importance for a wide variety of practical applications such as spray coating [1], pesticide deposition on plant leaves [2,3], inkjet printing [4], bioarray design [5], and so on. For most of these applications, one seeks to optimize the coverage of the liquid and/or to avoid losing any of the material contained in the impinging droplets. For the high-speed impact of droplets on different surfaces, an important open question remains for what gives the maximum coverage, i.e., the maximum radius that every impacting droplet attains. This question is also key for forensic bloodstain pattern analysis on crime scenes. The current methodology to determine where a victim was during the crime can be very inaccurate [6], as it is often not possible to determine the position of a victim, e.g., standing or sitting. This information can be crucial for the reconstruction of events which may refute or support the alibi of a suspect. The inaccuracies are caused by the straight-line approximation, because gravity and drag are not taken into account in the flight path of the blood drops. To take these forces into account, the impact velocity is required; a possible avenue is to try to determine this velocity from the size and volume of the bloodstains. Such an approach would allow for a much more accurate reconstruction of events, in contrast to the straight-line approximations that are currently used [7,8].

When a droplet hits the surface, it rapidly spreads in a circular fashion within several milliseconds [9]; see Fig. 1. Spreading is driven by the inertia of the droplet and countered by the capillary and viscous forces [10,11].

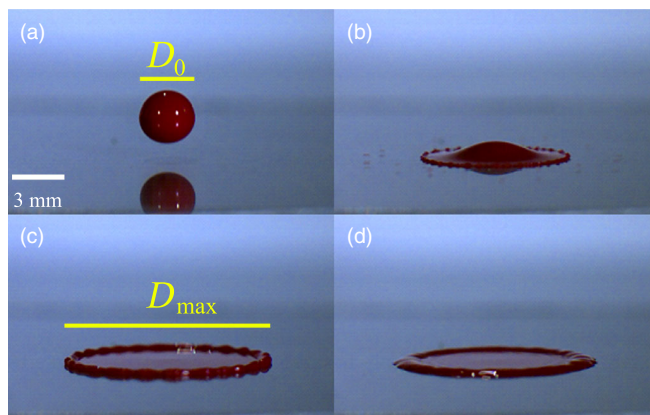


FIG. 1. (a)–(d) High-speed camera recording of a single blood droplet impacting ($v \approx 2$ m/s) on a stainless-steel substrate. (a) At 0.2 ms prior to droplet impact, the droplet is spherical. (b) At 0.6 ms after droplet impact on the surface, a thin lamella spreads outwards due to the inertial forces. (c) At 2.4 ms after droplet impact, the lamella increases in size. Spreading of the lamella slows down until it reaches its maximum size (D_{\max}), while there is a buildup of liquid in the outer rim. (d) At 4 ms after droplet impact, the bulk of the liquid is distributed over the entire stain.

In general, these forces are quantified in terms of the ratio between the inertial and capillary forces (the Weber number) $We \equiv \rho D_0 v^2 / \sigma$ or between the inertial and viscous forces (the Reynolds number) $Re \equiv \rho D_0 v / \eta$, where ρ denotes the density of the fluid, D_0 the diameter of the droplet in flight, v the impact velocity of the droplet, σ the surface tension, and η the viscosity of the fluid. A few milliseconds after impact, the spreading droplet reaches its maximum diameter D_{\max} , after which it can either retract due to the capillary forces [12] or remain pinned to the surface [2,13].

How the maximum diameter that the droplet attains varies with the experimental parameters remains a much-debated issue. Especially for the forensic application, to properly analyze bloodstain patterns, one needs to know the relation between the impact velocity, the stain size, and the volume of the droplet. A large number of different models have been proposed for the maximum radius; these use different arguments and sometimes arrive at very different conclusions [14,15]. Theory suggests that, when the spreading of a droplet is solely limited by viscous forces, the maximum spreading ratio D_{\max}/D_0 follows from equating the kinetic energy to the viscous dissipation and varies as $Re^{1/5}$ for $Re > 100$ [16,17]. However, in the forensic domain, one generally uses an impact-spreading model that predicts a scaling with $Re^{1/4}$ in the viscous regime [18], in contrast to the $Re^{1/5}$ scaling that was reported in several experimental studies [11,14,16,19–21].

Moreover, for the capillary regime (in which viscous forces are negligibly small), there is also an ongoing debate on two different scaling laws for the variation of the maximum diameter with impact speed. The first argument relies on energy conservation: If the kinetic energy of the drop is completely converted into surface energy of the pancakelike droplet after impact, D_{\max}/D_0 should scale as $We^{1/2}$ for $We > 100$ [22,23]. The second argument is

based on momentum and mass conservation, wherein the thickness of the spreading droplet at maximum extension is determined from an effective capillary length that takes into account the deceleration of the impacting droplet. This model predicts $D_{\max}/D_0 \propto We^{1/4}$, which has been reported in experiments [20,21,24] but sharply contrasts with the energy-conservation (EC) argument. In the forensic literature, even more complicated models attempt to obtain the impact velocity from the number of spines visible around the bloodstain [25–27] or by taking the splashing behavior of blood droplets into account [28]. These methods introduce multiple empirical constants, which severely limits their applicability. There is therefore a great necessity to establish the relation between the maximum diameter and the impact velocity by an objective method.

II. EXPERIMENT

In this paper, we study a large number of impact events under a variety of experimental circumstances. The results allow us to conclude that, in most practical situations (and notably those encountered in previous experiments that disagree on the scalings), We and Re have similar values, indicating that all three forces (inertial, viscous, and capillary) are important [29]. It is for this reason that neither simple viscous nor capillary scaling are observed. We propose a crossover scaling between the two regimes that collapses all of our (and previous) data, which shows that the asymptotically correct scaling in the capillary regime is $We^{1/2}$ and $Re^{1/5}$ in the viscous regime. In addition, we show that these results also hold when impact on inclined surfaces is considered, by simply taking into account only the component of the velocity that is perpendicular to the surface. We subsequently apply these results to blood droplets and show that these results allow us to deduce the

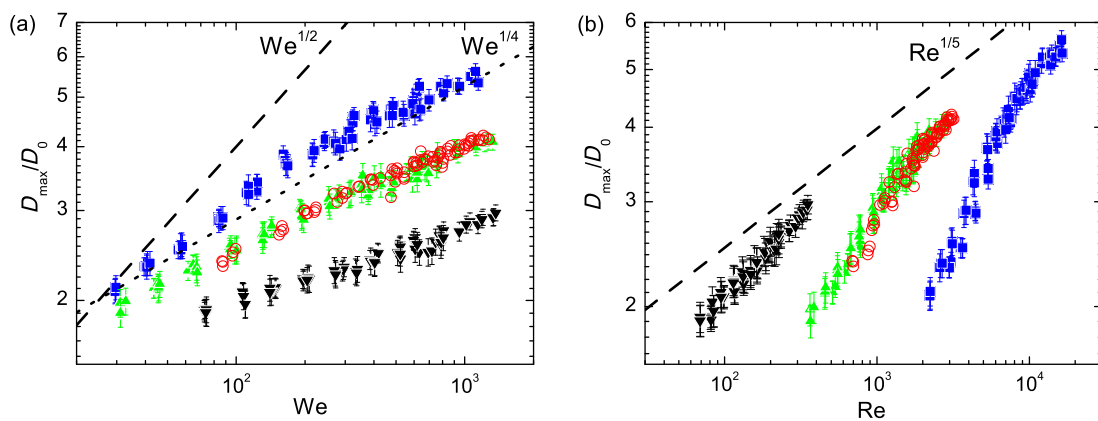


FIG. 2. Results for the impact experiments of single droplets of four kinds of liquid: water (squares), water-glycerol 6 mPa s (up triangles), water-glycerol 51 mPa s (down triangles), and blood (circles). Droplets are deposited on (rolled) stainless-steel surfaces with a contact angle between 80° and 90° for each fluid. The droplets have impact velocities between 0.9 and 5 m/s. (a) The maximum spreading ratio as a function of the Weber number, with scaling behavior $We^{1/2}$ (dashed line) and $We^{1/4}$ (dotted line) depicted for comparison. (b) The maximum spreading ratio as a function of the Reynolds number, with scaling behavior $Re^{1/5}$ (dashed line). The errors depicted in (a) and (b) are due to the uncertainty in determining D_{\max} and D_0 .

impact velocity from bloodstains based on the size and volume, regardless of the impact angle and wetting properties of the solid surface, which is a major advance in forensic bloodstain pattern analysis.

Experiments are done with simple fluids with a range of different viscosities ($1 \text{ mPa}\cdot\text{s} \leq \eta \leq 51 \text{ mPa}\cdot\text{s}$): water, two water-glycerol mixtures, and blood as a shear-thinning fluid. Shear thinning is the most prominent and most important non-Newtonian effect for complex fluids; it has been shown that elastic effects such as normal stresses [30] have no influence on the maximum droplet diameter [12]. The viscosity is determined with a stress-controlled rheometer (Anton Paar, MCR 302, Graz, Austria), the surface tension and contact angles are determined by means of the pendant-drop method, and the contact angle is determined with the sessile-drop method (EasyDrop, Kruss, Hamburg, Germany). For the physical properties of the used liquids, see Ref. [31]. A high-speed camera (Phantom v7.1, Vision research) is used to record the impact of the droplets generated by using a syringe pump (droplet volume between 5 and 20 μl). The impact velocity is changed by varying the fall height ($0.5 \text{ m/s} < v < 6 \text{ m/s}$). From the high-speed recordings, the size of the droplet (D_0) and the maximum spreading diameter (D_{max}) are measured, by means of a reference length. The spreading ratio D_{max}/D_0 is plotted as a function of both the Weber [Fig. 2(a)] and the Reynolds number [Fig. 2(b)]. Even though the $We^{1/4}$ scaling seems consistent with water, it is not for blood or water-glycerol. Moreover, it is clear that the data points for the different systems do not overlap, excluding a simple scaling with either of the two parameters; none of our data sets can be convincingly rescaled with the dependencies ($Re^{1/5}$, $Re^{1/4}$, $We^{1/2}$, $We^{1/4}$) reported in the literature (Fig. 2).

III. SCALING OF THE MAXIMUM SPREADING DIAMETER

A. Spreading model

The fact that no clear dependency on We or Re is found suggests that all three forces mentioned above (inertial, capillary, and viscous) are important. In fact, there may be a broad crossover regime between the viscous and capillary regimes. To test this possibility, we adopt the approach of Eggers *et al.* [23] by interpolating between the $We^{1/2}$ and $Re^{1/5}$ scaling by using

$$D_{\text{max}}/D_0 \propto Re^{1/5} f_{\text{EC}}(WeRe^{-2/5}), \quad (1)$$

where f_{EC} is a function of the parameter $WeRe^{-2/5}$ that varies between zero (capillary regime) and infinity (viscous regime). For the momentum-conservation (MC) model [20], we interpolate between the $We^{1/4}$ and $Re^{1/5}$ scaling by using

$$D_{\text{max}}/D_0 \propto Re^{1/5} f_{\text{MC}}(WeRe^{-4/5}), \quad (2)$$

where f_{MC} is a function of the parameter $WeRe^{-4/5}$. For the energy-conservation model based on $We^{1/2}$, this procedure indeed succeeds in collapsing all data points for different liquids and impact velocities onto one single curve [Fig. 3(a)]. Notably, using the momentum-conservation model does not result in collapsing the data points onto one single curve [see Fig. 3(b)], from which we can deduce that $We^{1/4}$ is not the correct scaling behavior for the capillary regime. Our results show that droplet spreading upon impact is dominated by inertial, viscous, and capillary forces; energy dissipation at the substrate-liquid interface and energy transfer into internal flows marginally hinder droplet spreading. To emphasize the strength of our approach, we also successfully revisit earlier data of water-glycerol mixtures from Bartolo, Josserand, and Bonn [21], whose target surface is nonwetting (Fig. 3).

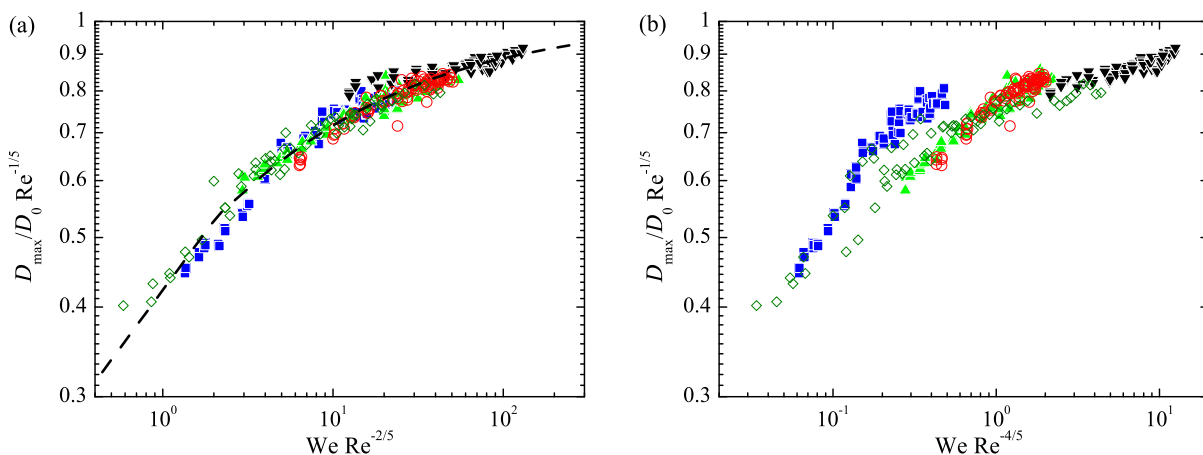


FIG. 3. (a) The rescaled maximum spreading ratio as a function of $WeRe^{-2/5}$, with the dashed line showing the Padé approximant function [Eq. (3)] fitted to the data points. (b) The rescaled maximum spreading ratio as a function of $WeRe^{-4/5}$. To emphasize the strength of our approach, we also successfully revisit earlier data of water-glycerol mixtures from Bartolo, Josserand, and Bonn [21] (diamonds). For reasons of clarity, the errors are not shown.

In all of these experiments, we find that any decrease in volume due to splashing (the ejection of microscopic droplets) is negligible, and we do not observe any deviations from the proposed scaling; in our experiments, splashing does not affect the maximum diameter scaling.

To quantitatively relate the maximum spreading ratio to the impact velocity, we exploit the existence of a one-variable scaling function, $f_{\text{EC}}(\text{WeRe}^{-2/5})$. We first introduce the impact parameter $P \equiv \text{WeRe}^{-2/5}$ to distinguish between the two asymptotic regimes where the physical mechanisms that compete are clearly identified. In the high-viscosity limit, the relation $D_{\text{max}}/D_0 \propto \text{Re}^{1/5}$ implies that $f_{\text{EC}}(P) \sim 1$ in the limit $P \gg 1$. Conversely, when $P \ll 1$, f_{EC} has to scale as $f_{\text{EC}}(P) \propto P^{1/2}$ in order to recover the inviscid $D_{\text{max}}/D_0 \propto \text{We}^{1/2}$ scaling. The smooth crossover between these two asymptotics is then constructed by using a so-called [1,1] Padé approximant [32], which is a ratio of two first-order polynomials that approximates the actual function f_{EC} :

$$(D_{\text{max}}/D_0)\text{Re}^{-1/5} = P^{1/2}/(A + P^{1/2}), \quad (3)$$

where $A = 1.24 \pm 0.01$ is a fitting constant obtained by means of a least-squares fit (with the coefficient of determination $R^2 = 0.95$). To check for robustness, we also use the “least-absolute-deviations” method to determine A , which does not significantly deviate from 1.24 [33]. The fit of Eq. (3) agrees excellently with the data [Fig. 3(a)], thereby confirming that no other physical principle but energy conservation is required to account for droplet spreading. When fitting the momentum-conservation model ($P = \text{WeRe}^{-4/5}$) with a Padé approximant, the fitting is significantly worse ($R^2 = 0.83$), which echoes the poor rescaling of our data in Fig. 3(b). We do not obtain better results by fitting other functions or higher-order Padé approximants. The analytical solution describes the spreading behavior of various different fluids, thus yielding a quantitative relation between the impact velocity and maximum spreading ratio over a large range of Weber and Reynolds numbers ($10 < \text{We} < 1700$ and $70 < \text{Re} < 17000$).

B. Non-Newtonian properties of blood

Blood has non-Newtonian shear-thinning properties [34], but the above results [Fig. 4(a)] show that our data for blood also fall onto the universal curve. This result means that blood spreads similarly to a Newtonian fluid with similar viscosity. For the agreement, the high-shear viscosity is taken: $\eta_{\text{inf}} = 4.8 \text{ mPa s}$ [Fig. 4(b)], which seems reasonable in view of the high deformation rates involved in this experiment. This result therefore solves the hydrodynamic problem, but for the forensic application yet another question has to be answered: How does the maximum diameter just after impact compare to the size of a dried-up bloodstain? It turns out that the two are identical, since the contact line of the blood drop remains pinned onto the surface after reaching the maximum diameter. This pinning happens for a wide variety of impact conditions

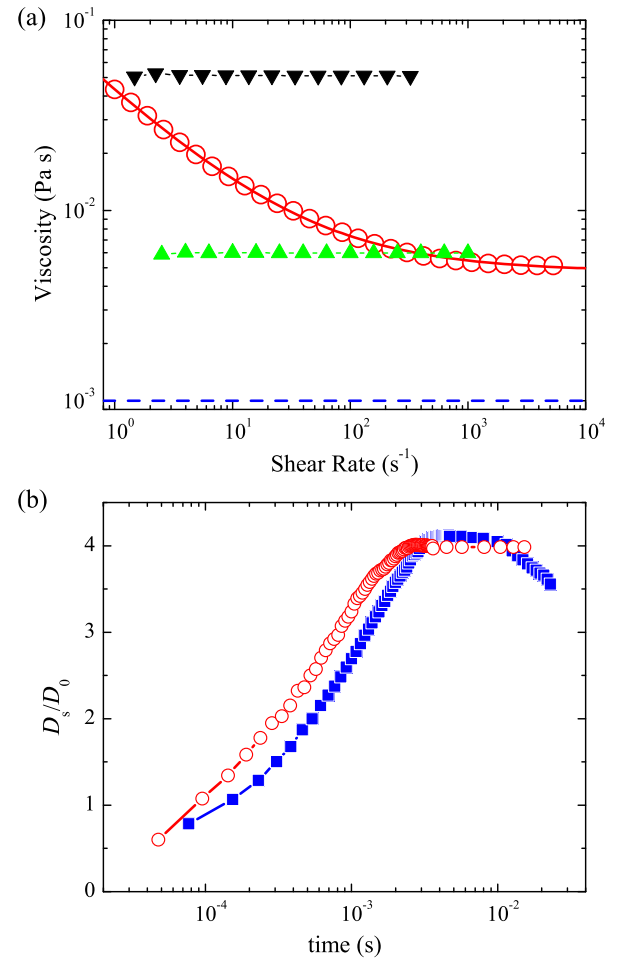


FIG. 4. (a) Viscosity as a function of the shear rate of the two water-glycerol mixtures (triangles) and blood (circles), with water as a reference (dashed line). The shear-thinning effect of blood (at 37.5 °C) is clear, as the viscosity decreases as a function of shear rate. For high shear rates, the viscosity reaches a constant, which is determined by means of fitting $\eta = \eta_{\text{inf}} + k\gamma^{n-1}$ to the data points (red line), from which we obtain a high shear-rate viscosity of $\eta_{\text{inf}} = 4.8 \text{ mPa s}$; $k = 38 \text{ mPa s}^n$ and $n = 0.41$ are fitting constants. (b) The spreading ratio D_s/D_0 (D_s is the spreading diameter as a function of time) of water (squares) and blood (circles) droplets during impact. Water retracts after reaching its maximum diameter, while blood does not, which pins to the surface (stainless steel).

and surfaces, discussed below. Figure 4(a) shows a typical trace of the diameter of the bloodstain in time that examines whether the blood retracts from the surface after deposition (as water does on a hydrophobic surface); the blood drop remains perfectly anchored onto the surface. The diameter of the dried bloodstain thus equals D_{max} , and consequently dried bloodstains found at the crime scene contain useful information about the impact speed.

C. Impact on inclined surfaces

So far, we have considered droplets falling perpendicularly onto a stainless-steel surface. To investigate the

generality of our findings, we need to consider (a) different surfaces and (b) different impact angles; the latter since, in most situations of practical relevance, the impact is not perpendicular. On inclined surfaces, (blood)stains are often elliptically shaped, with short axis W_{\max} and long axis L_{\max} , empirically related to the impact angle α through $W_{\max}/L_{\max} = \sin \alpha$ [35]. We therefore deposit droplets (water and blood) onto different types of surfaces and with different inclinations between 10° and 90° . For larger droplets and steeply inclined surfaces, we observe that the liquid may continue to flow along the surface after the impact event, thereby increasing its length [36]. We therefore consider here only the extension of the fluid along the short axis as the relevant parameter for determining the maximum extension.

The impact velocity can be divided into a component parallel and perpendicular with respect to the surface, $v_{\parallel} = v_{\text{impact}} \cos \alpha$ and $v_{\perp} = v_{\text{impact}} \sin \alpha$, respectively [28]. For spreading along the short axis, we take only the perpendicular component of the velocity into account. Accordingly, Eq. (3) can be rewritten as

$$W_{\max}/D_0 = \text{Re}^{1/5} \frac{P^{1/2} \sin \alpha}{[A + P^{1/2}(\sin \alpha)^{4/5}]}, \quad (4)$$

allowing for the same rescaling. We find that the relations uncovered above still hold for different and for inclined surfaces [37].

D. Determining impact velocity from maximum spreading

For the forensic application of our results, we test whether the impact velocity of a bloodstain can indeed be determined *accurately* by means of our method. Accordingly, we compare the impact velocities measured directly from the high-speed camera footage with those calculated from Eq. (4) based on the width, the volume, and the impact angle of the stains. Figure 5(a) shows very good agreement between measured and calculated velocities. This agreement illustrates that the proposed relation can be successfully used to determine the impact velocity of a blood droplet from a dried bloodstain. For the inclined surfaces, as is clear from Fig. 5(b) for all impact angles, there is also a very good agreement between the measured and calculated velocities. The data points from Figs. 5(a) and 5(b) are normally distributed around the $x = y$ line (the mean of the calculated velocity divided by the measured velocity is 1.004) with a standard deviation of 10%. Accordingly, with our universal relation it is possible to determine the maximum spreading ratio accurately. In addition, the impact velocity can be determined by means of the width, the volume, and the impact angle of a bloodstain. Moreover, the variation in surface does not significantly influence the velocity estimation for blood droplets.

To apply our findings to the crime scene for bloodstain pattern analysis, it is, however, necessary to determine what

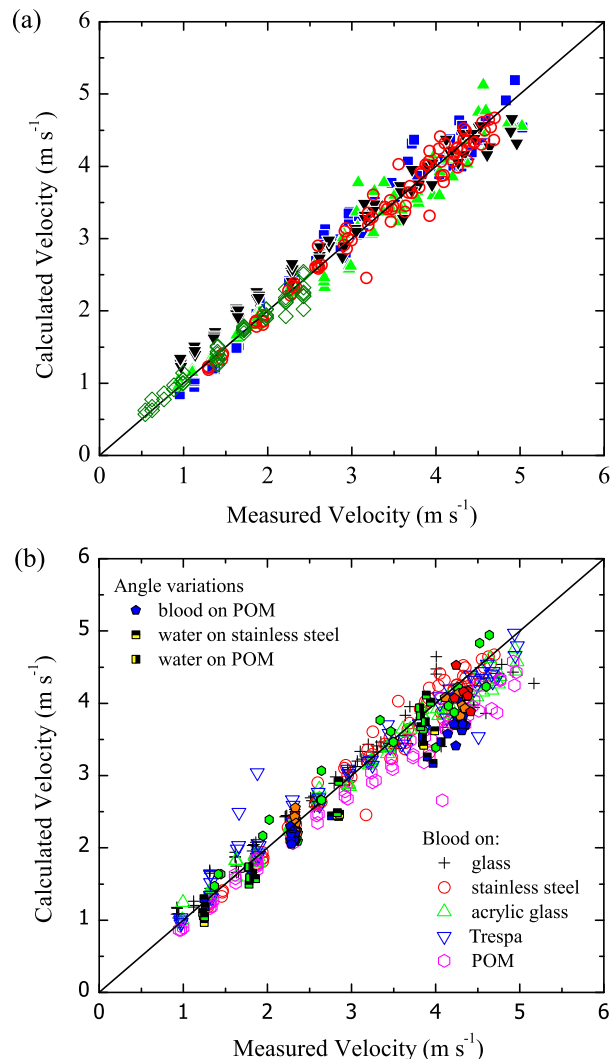


FIG. 5. Calculated impact velocity versus measured impact velocity. (a) The impact velocity is calculated by solving Eq. (4) numerically based on the volume and maximum spreading ratio for water, water-glycerol mixtures (including the data of Bartolo, Josserand, and Bonn [21]), and blood falling onto stainless-steel surfaces with an impact angle of 90° . (b) Blood falling onto various surfaces (POM is polyoxymethylene). Water and blood deposited on POM and stainless steel with varying impact angles (filled symbols): $\alpha \leq 25^\circ$ (blue), $25^\circ < \alpha \leq 40^\circ$ (green), $40^\circ < \alpha \leq 65^\circ$ (yellow), $65^\circ < \alpha \leq 75^\circ$ (orange), and $75^\circ < \alpha \leq 90^\circ$ (red). The static contact angles for the surfaces with water are glass $\theta = 20^\circ \pm 2^\circ$, stainless steel $\theta = 90^\circ \pm 5^\circ$, acrylic glass $\theta = 70^\circ \pm 2^\circ$, Trespa $\theta = 82^\circ \pm 3^\circ$, and POM $\theta = 79^\circ \pm 2^\circ$.

the original droplet volume is from a dried stain. A recent study has shown how to determine the volume of a dried bloodstain and infer the original droplet volume by means of optical coherence tomography [38].

IV. CONCLUSION

In conclusion, we show that a universal solution can be used to describe the impact behavior of fluids on solid

substrates in the crossover regime between capillary and viscous regimes, which covers most practical situations. Thereby, resolving a long-standing problem within the fluid dynamical community, namely, that the spreading behavior for the capillary and viscous regimes is solely governed by energy conservation. We show that it is possible to determine the impact velocity of a blood droplet from the size of the bloodstain on different surfaces as well as for various impact angles in an objective manner. We anticipate this particular finding to be of considerable importance for investigators who use bloodstain pattern analysis to reconstruct the events that have taken place at crime scenes. This method allows for an accurate reconstruction of the flight trajectories of the blood droplets and will allow one, for example, to better determine the position of the victim or to connect bloodstain patterns to specific wounds on the body, which differ in height. Such information is crucial in the court of law considering the reconstruction of events which could lead to either the conviction or the acquittal of a suspect. In addition, this method opens up the possibility to connect bloodstain pattern formation to the manner and, more specifically, force of creation. More generally, the results of this study may be used over a wider range of industrial applications for which the control of droplet deposition is of prominent importance [1–4].

This research is supported by the Dutch Technology Foundation STW, which is part of the Netherlands Organisation for Scientific Research (NWO) and which is partly funded by the Ministry of Economic Affairs, Agriculture and Innovation. We thank Kevin Liebrand, Nils Vollenhoven, and Katharina Baron for their experimental contributions and Joost van Marmeren for advice.

-
- [1] S. D. Aziz and S. Chandra, Impact, recoil and splashing of molten metal droplets, *Int. J. Heat Mass Transfer* **43**, 2841 (2000).
 - [2] V. Bergeron, D. Bonn, J. Y. Martin, and L. Vovelle, Controlling droplet deposition with polymer additives, *Nature (London)* **405**, 772 (2000).
 - [3] W. Wirth, S. Storp, and W. Jacobsen, Mechanisms controlling leaf retention of agricultural spray solutions, *Pesticide science* **33**, 411 (1991).
 - [4] B.-J. deGans, P. C. Duineveld, and U. S. Schubert, Inkjet printing of polymers: State of the art and future developments, *Adv. Mater.* **16**, 203 (2004).
 - [5] M. J. Heller, DNA microarray technology: Devices, systems, and applications, *Annu. Rev. Biomed. Eng.* **4**, 129 (2002), PMID 12117754.
 - [6] K. G. de Bruin, R. D. Stoel, and J. C. M. Limborgh, Improving the point of origin determination in bloodstain pattern analysis, *J. Forensic Sci.* **56**, 1476 (2011).
 - [7] I. H. L. MacDonell, *Bloodstain Patterns*, 37th ed. (Golos, New York, 1993).

- [8] A. L. Carter, The directional analysis of bloodstain patterns—Theory and experimental validation, *Can. Soc. Forensic Sci. J.* **34**, 173 (2001).
- [9] See Supplemental Material at <http://link.aps.org/supplemental/10.1103/PhysRevApplied.2.044018> for a high-speed camera recording of a single blood droplet impacting on a stainless-steel substrate.
- [10] H. Marmanis and S. T. Thoroddsen, Scaling of the fingering pattern of an impacting drop, *Phys. Fluids* **8**, 1344 (1996).
- [11] I. V. Roisman, R. Rioboo, and C. Tropea, Normal impact of a liquid drop on a dry surface: Model for spreading and receding, *Proc. R. Soc. A* **458**, 1411 (2002).
- [12] D. Bartolo, A. Boudaoud, G. Narcy, and D. Bonn, Dynamics of non-Newtonian droplets, *Phys. Rev. Lett.* **99**, 174502 (2007).
- [13] B. L. Scheller and D. W. Bousfield, Newtonian drop impact with a solid surface, *AIChE J.* **41**, 1357 (1995).
- [14] M. Rein, Phenomena of liquid drop impact on solid and liquid surfaces, *Fluid Dyn. Res.* **12**, 61 (1993).
- [15] S. M. An and S. Y. Lee, Maximum spreading of a shear-thinning liquid drop impacting on dry solid surfaces, *Exp. Therm. Fluid. Sci.* **38**, 140 (2012).
- [16] J. Madejski, Solidification of droplets on a cold surface, *Int. J. Heat Mass Transfer* **19**, 1009 (1976).
- [17] S. Chandra and C. T. Avedisian, On the collision of a droplet with a solid surface, *Proc. R. Soc. A* **432**, 13 (1991).
- [18] M. Pasandideh-Fard, R. Bhole, S. Chandra, and J. Mostaghimi, Deposition of tin droplets on a steel plate: Simulations and experiments, *Int. J. Heat Mass Transfer* **41**, 2929 (1998).
- [19] G. Trapaga and J. Szekeley, Mathematical modeling of the isothermal impingement of liquid droplets in spraying processes, *Metall. Mater. Trans. B* **22**, 901 (1991).
- [20] C. Clanet, C. Béguin, D. Richard, and D. Quéré, Maximal deformation of an impacting drop, *J. Fluid Mech.* **517**, 199 (2004).
- [21] D. Bartolo, C. Josserand, and D. Bonn, Retraction dynamics of aqueous drops upon impact on non-wetting surfaces, *J. Fluid Mech.* **545**, 329 (2005).
- [22] T. Bennett and D. Poulikakos, Splat-quench solidification: Estimating the maximum spreading of a droplet impacting a solid surface, *J. Mater. Sci.* **28**, 963 (1993).
- [23] J. Eggers, M. A. Fontelos, C. Josserand, and S. Zaleski, Drop dynamics after impact on a solid wall: Theory and simulations, *Phys. Fluids* **22**, 062101 (2010).
- [24] P. Tsai, M. H. W. Hendrix, R. R. M. Dijkstra, L. Shui, and D. Lohse, Microscopic structure influencing macroscopic splash at high Weber number, *Soft Matter* **7**, 11325 (2011).
- [25] N. Z. Mehdizadeh, S. Chandra, and J. Mostaghimi, Formation of fingers around the edges of a drop hitting a metal plate with high velocity, *J. Fluid Mech.* **510**, 353 (2004).
- [26] L. Hulse-Smith, N. Z. Mehdizadeh, and S. Chandra, Deducing drop size and impact velocity from circular bloodstains, *J. Forensic Sci.* **50**, 1 (2005).
- [27] C. Knock and M. Davison, Predicting the position of the source of blood stains for angled impacts, *J. Forensic Sci.* **52**, 1044 (2007).
- [28] C. D. Adam, Fundamental studies of bloodstain formation and characteristics, *Forensic Sci. Int.* **219**, 76 (2012).

- [29] For example, taking a blood droplet with a diameter of 2 mm and an impact velocity of 4 m/s will result in a Weber and Reynolds number of roughly 562 and 1688, respectively.
- [30] D. Bonn and J. Meunier, Viscoelastic free-boundary problems: Non-Newtonian viscosity vs normal stress effects, *Phys. Rev. Lett.* **79**, 2662 (1997).
- [31] See Supplemental Material at <http://link.aps.org/supplemental/10.1103/PhysRevApplied.2.044018> for the physical properties of the used liquids.
- [32] W.H. Press, S.A. Teukolsky, W.T. Vetterling, and B. Flannery, *Numerical Recipes: The Art of Scientific Computing*, 3rd ed. (Cambridge University Press, Cambridge, England, 2007).
- [33] See Supplemental Material at <http://link.aps.org/supplemental/10.1103/PhysRevApplied.2.044018> for the least-absolute-deviations method.
- [34] E. W. Merrill, Rheology of blood, *Physiol. Rev.* **49**, 863 (1969), <http://physrev.physiology.org/content/49/4/863>.
- [35] V. Balthazard, R. Piédélièvre, H. Desoille, and L. Dérobert, Étude des gouttes de sang projeté, *Ann. Med. Leg. Criminol. Police Sci. Med. Soc. Toxicol.* **19**, 265 (1939).
- [36] See Supplemental Material at <http://link.aps.org/supplemental/10.1103/PhysRevApplied.2.044018> for a high-speed recording of a single blood droplet impacting on an inclined surface.
- [37] See Supplemental Material at <http://link.aps.org/supplemental/10.1103/PhysRevApplied.2.044018> for the spreading behavior of water and blood on inclined POM surfaces.
- [38] N. Laan, R. H. Bremmer, M. C. G. Aalders, and K. G. de Bruin, Volume determination of fresh and dried bloodstains by means of optical coherence tomography, *J. Forensic Sci.* **59**, 34 (2014).